JOURNAL OF GEOPHYSICAL RESEARCH, VOL. 104, NO. A2, PAGES 2459–2475, FEBRUARY 1, 1999

# Case studies on the wave propagation and polarization of ELF emissions observed by Freja around the local proton gyrofrequency

Ondřej Santolík[1]

Faculty of Mathematics and Physics, Charles University, Prague, Czech Republic

Michel Parrot

Laboratoire de Physique et Chimie de l'Environnement, Centre National de la Recherche Scientifique, Orléans, France

**Abstract.** Using a multicomponent measurement of electric and magnetic fields in the ELF range, we investigate the polarization and propagation characteristics of several types of electromagnetic emissions around the local proton gyrofrequency. The data of the low-orbiting Freja satellite are examined in the auroral and subauroral regions as well as inside the plasmasphere. We confirm previous results on the properties of the high-latitude hiss with a sharp lower cutoff just below the local proton gyrofrequency. The waves propagate downward from higher altitudes outside the plasmasphere and reflect at the local two-ion cutoff frequency. With an enhanced data representation we are able to characterize the reflected upgoing waves on both poleward and equatorward edges of the hiss emission. The high-latitude emissions in a large band below the local proton gyrofrequency contain right-hand circularly polarized waves propagating nearly parallel to the terrestrial magnetic field. We believe these emissions can originate by tunnelling of the right-hand-polarized hiss below the two-ion crossover frequency. We report high-latitude "frequency drift phenomena" below the local proton gyrofrequency. The frequency of these faint emissions increases by several tens of hertz per latitude degree. The electromagnetic noise at low frequencies is always found with a high degree of a nearly linear polarization. Upgoing ion whistlers are observed to follow each other with time delays as low as about 100 ms.

## 1. Introduction

Several different types of ELF wave phenomena have been reported by low-orbiting satellites at high and middle latitudes. A broadband electromagnetic noise is often observed in the auroral region [*Gurnett et al.*, 1984]. Its intensity is maximum at low frequencies (below the local oxygen gyrofrequency) and gradually decreases toward higher frequencies. The emissions sometimes extend up to the local proton gyrofrequency ($f_{\mathrm{H}+}$), especially in the electric field component. Associated broadband electrostatic waves can be observed up to 2 kHz [*Wahlund et al.*, 1994]. The authors identified these waves as ion acoustic mode and believe them to be triggered by solitary kinetic Alfvén waves. The connection of the broadband noise to the Alfvén resonance cones in an inhomogeneous plasma is examined by *Stasiewicz et al.* [1997]. These phenomena, associated with the low-density cavities, are believed to play an important role in the auroral plasma processes.

Extensive attention has been paid to narrowbanded waves below $f_{\mathrm{H}+}$ [e.g., *Gurnett and Frank*, 1972; *Temerin and Lysak*, 1984; *Saito et al.*, 1987; *Gustafsson et al.*, 1990]. The emissions are observed mainly between the local proton and helium gyrofrequencies and occur mostly in the premidnight sector at auroral latitudes [*Saito et al.*, 1987]. It is widely accepted that these waves are generated by inverted-V electrons in the auroral acceleration region, as proposed by *Temerin and Lysak* [1984]. Analysis of the wave polarization based on a Freja observation [*Oscarsson et al.*, 1997] shows that the wave vector direction is nearly perpendicular to the Earth's magnetic field $\mathbf{B}_0$, as predicted by the above generation mechanism. In contrast with other types of emissions, there are very few studies on a large class of auroral emissions below $f_{\mathrm{H}+}$, which are not strictly narrowbanded but have a lower frequency limitation of both electric and magnetic spectra. A statistical analysis of a large set of Freja observations shows that the wave vector direction is rather field-aligned [*Santolík and Parrot*, 1998]. The waves propagate downward in the right-hand-polarized mode, and their phase velocity is in agreement with the cold plasma theory. The emissions occur on the dayside, with the maximum wave power near the local noon. Some of these properties have been previously indicated by two case studies based on the Aureol 3 data [*Rauch et al.*, 1985; *Lefeuvre et al.*, 1992].

The ELF hiss above $f_{\mathrm{H}+}$ has been reported by many papers in the past. Its sharp lower cutoff near $f_{\mathrm{H}+}$ has been first explained by *Gurnett and Burns* [1968]. *Muzzio and Angerami* [1972] observed hiss emissions limited to a frequency band above $f_{\mathrm{H}+}$. Generation models are generally based on the electron cyclotron instability [e.g., *Solomon et al.*, 1988]. The direction of the Poynting vector of the hiss has been determined using Injun 5 measurements [*Mosier*, 1971]. Extensive studies on the wave propagation of the ELF hiss have been done using the Aureol-3 measurements [*Rauch et al.*,

[1] Also at Institute of Atmospheric Physics, Academy of Sciences of the Czech Republic, Prague.



Paper number JGRA-1998900045.
0148-0227/02/JGRA-1998900045$9.00

1985; *Hayakawa et al.*, 1985; *Lefeuvre et al.*, 1992]. In the latter paper, the direct evidence on the hiss reflection, and the simultaneous observation of downgoing and reflected upgoing waves have been reported. *Rauch et al.* [1993] underlined the efficiency of the waves close to $f_{\mathrm{H}+}$ in the formation of $\mathrm{H}^+$ conics.

The aim of the present paper is to show an overview of the propagation and polarization characteristics of various ELF electromagnetic emissions observed by the low-altitude satellite Freja around $f_{\mathrm{H}+}$. We have processed about 70 randomly chosen passes over the northern auroral and subauroral regions, and according to different appearances in frequency-time spectrograms, we have classified the observations into six distinct groups. Type A: Auroral ELF hiss emissions with a sharp lower cutoff just below $f_{\mathrm{H}+}$ [*Gurnett and Burns*, 1968]. The waves are clearly electromagnetic, in distinction from the nearly electrostatic auroral hiss above the lower hybrid frequency ($f_{\mathrm{lh}}$). The emissions sometimes go up only to several hundreds of Hz above $f_{\mathrm{H}+}$, but they can also extend to several kHz. Type B: Narrowbanded auroral ELF emissions below $f_{\mathrm{H}+}$ [*Gurnett and Frank*, 1972; *Temerin and Lysak*, 1984; *Saito et al.*, 1987; *Gustafsson et al.*, 1990; *Oscarsson et al.*, 1997]. Type C: Auroral ELF emissions below $f_{\mathrm{H}+}$ with lower-frequency limitation [*Rauch et al.*, 1985; *Lefeuvre et al.*, 1992; *Santolík and Parrot*, 1998]. The frequency band is wider ($\Delta f > \frac{1}{4} f_{\mathrm{H}+}$), and there is not necessarily a stop-band below $f_{\mathrm{H}+}$. Some events of this type have a sharp lower cutoff around or below $\frac{1}{4} f_{\mathrm{H}+}$, but a diffuse and fluctuating lower frequency limit is also often seen. The "type A" hiss is often associated. Type D: A broadband electromagnetic noise similar to the observations of *Gurnett et al.* [1984], *Wahlund et al.* [1994], and *Stasiewicz et al.* [1997]. The wave intensity gradually fades out at higher frequencies. The emissions can go up to $f_{\mathrm{H}+}$ and even higher, especially in the electric field spectrum. Type E: Emissions with a clear upper cutoff at $f_{\mathrm{H}+}$, observed at lower magnetic latitudes (below about 55°). Waves having an upper cutoff at the local helium gyrofrequency ($f_{\mathrm{He}+}$) are often associated. Type F: Waves at lower latitudes (below about 55°) with a lower cutoff similar to the type A, but located several tens of hertz below $f_{\mathrm{H}+}$. The difference compared to the type A also lies in frequent presence of a weak diffuse band below the main cutoff. The spectral power density in this band is by 1 or 2 orders lower than above the main cutoff. The main hiss emission is often limited to a band of several hundreds of hertz above $f_{\mathrm{H}+}$ [*Muzzio and Angerami*, 1972] or an internal stop-band is observed [*Rauch et al.*, 1985].

As far as we know, Aureol 3 and Freja are the only two polar-orbiting satellites at low altitudes which made systematic waveform measurements of the magnetic field vector in the ELF range, together with the waveform of at least one electric field component. These data allow a detailed analysis of the wave polarization. In the set of 70 Freja passes we have checked the correspondence of the above spectral types to wave polarization and propagation characteristics. In this paper we present the results for three representative passes containing all the emission types A-F. We restrict ourselves to the determination of several parameters with a relatively obvious definition, such as the wave vector direction and the ellipticity of the wave polarization. To represent these parameters, we chose an unusual way of spectrogram-like images, which allows an overall view of the time-frequency evolution. We do not attempt to determine the wavelengths associated with the emissions [e.g., *Walker et al.*, 1991], neither we estimate more complex wave characteristics such as the wave distribution functions [*Storey and Lefeuvre*, 1974, 1979, 1980].

In section 2 we will briefly describe the data and the methods which are used to find their characteristics. Examples of properties of the six spectral types will be given in section 3. These results will be discussed in section 4 and a comparison will be done with previous studies, in particular with the data analysis of *Rauch et al.* [1985], *Hayakawa et al.* [1985], and *Lefeuvre et al.* [1992] concerning the satellite Aureol 3. Brief conclusions will be given in section 5. Appendix contains a detailed description of our method to recognize upgoing and downgoing waves.

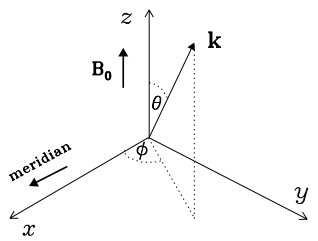


**Figure 1.** Spherical coordinate system connected with the terrestrial magnetic field $\mathbf{B}_0$ and with the local magnetic meridian.

## 2. Data

The satellite Freja was launched on October 6, 1992. The parameters of the orbit are inclination, 63°; apogee, 1756 km; perigee, 601 km; and period, 109 min. The satellite was spin stabilized with a spin period of about 6 s. The Freja mission was devoted to particle and field studies and auroral imaging at high latitudes (for details, see the special issue of *Space Science Reviews*, 70, 3/4, 1994). The wave experiment is described by *Holback et al.* [1994]. The device collects waveforms of electric and magnetic fields and plasma density in four frequency ranges: DC, LF (up to 2 kHz), MF (up to 16 kHz), and HF (up to 4 MHz). Four channels are recorded in the LF frequency range we use in this paper. Various combinations are possible, and for this study we have selected passes where three orthogonal magnetic components are measured by search-coil sensors, simultaneously with one electric component provided by a pair of spherical probes mounted on 10.6-m wire booms. The important point is that the systematically measured data are not continuously recorded.

The measurements are made in snapshots of various lengths and at various intervals depending on the different modes of the experiment. This matter is taken into account in our signal analysis in such a way that samples from adjacent snapshots are never mixed during the data processing. The data are mainly recorded at high latitudes when the satellite is visible to one of two ground stations: Esrange in Kiruna (Sweden) and Prince Albert (Canada).

Our analysis is carried out in a coordinate system linked to the local Earth's magnetic field $\mathbf{B}_0$: the $z$ axis lies along $\mathbf{B}_0$, the $x$ axis points toward the direction of decreasing magnetic latitude in the local magnetic meridian plane, and the $y$ axis completes the orthogonal set. In this system, the direction of the wave vector ($\mathbf{k}$) is characterized by the polar angle $\theta$ and the azimuthal angle $\phi$ (see Figure 1). We transform the three-axial magnetic field measurement to obtain the magnetic components in the above frame of reference. The local measurement of $\mathbf{B}_0$, necessary for these coordinate transformations is obtained from the Freja fluxgate magnetometer [*FREJA Magnetic Field Experiment Team*, 1994]. In a given time interval, the transformed waveforms are used to calculate the autopower and cross-power spectra. At a given frequency, these spectra form together a Hermitian spectral matrix. We obtain several wave parameters from the spectral matrix of the three magnetic components. The degree of polarization is estimated by the method of *Samson and Olson* [1980]. If the degree of polarization is equal to 1, the field components are mutually coherent, and the wave field is polarized in a single plane. This is consistent with the presence of a single plane wave in a single wave mode. For lower values of the polarization degree, the plane wave hypothesis becomes invalid. Note that for different types of plasma waves, a given value of the polarization degree could reflect different degrees of corruption of the plane wave hypothesis [*Pinçon et al.*, 1992]. Note also that the spectral analysis has a finite frequency resolution. A polarization degree near to 1 may then correspond to a superposition of plane

waves having the same propagation direction but occupying a finite interval of wavelengths. The possible extent of this interval depends on the wave dispersion of a given plasma mode. Note finally that values of the polarization degree could be influenced by the method of the spectral analysis (the number of averaged FFTs used to get the spectral matrix). This influence is, however, not of great practical importance since we compare values obtained by the same procedure.

The ellipticity of the magnetic field polarization is estimated from the eigenvector associated to the nonnull eigenvalue of the magnetic spectral matrix supposing the validity of the plane wave hypothesis [*Samson and Olson*, 1980]. The zero value implies a linear polarization, and the value of 1 corresponds to a circular polarization. The determination of the sense of polarization in the plane perpendicular to $\mathbf{B}_0$ is based on the sign of the imaginary part of the cross-spectrum between the $B_x$ and $B_y$ components [*Lefeuvre et al.*, 1986]. If this sign is positive, the waves are right-hand polarized, if it is negative, the waves are left-hand polarized. The method of *Means* [1972] is used to determine the $\mathbf{k}$ direction. This method is based on the imaginary part of the magnetic spectral matrix and gives correct values only when the plane wave approximation is valid. For a linear polarization, no result is provided and for waves with low ellipticities, the obtained values are influenced by large experimental errors due to uncertainties of the spectral matrix estimation. The method does not take into account the electric field measurements and thus is not able to distinguish between two antiparallel directions, $\mathbf{k}$ and $-\mathbf{k}$. To define $\theta$ and $\phi$ values we suppose waves having $k_z > 0$ ($k_z$ is the $z$-component of the wave vector, see Figure 1), and thus we always obtain $\theta \leq 90°$. This corresponds to the propagation toward the Earth (downward) in the northern hemisphere where all Freja data were recorded. If we, however, recognize by another method the waves are upgoing, we must shift the corresponding $\phi$ by 180°, and mirror the $\theta$ value to the hemisphere with $k_z < 0$. Obviously, interpretation of the results on the wave vector direction needs prior recognition of upgoing and downgoing waves. To do this, we have developed a procedure based on the electric field data provided by a single spinning antenna, and on a simultaneous measurement of the full magnetic field vector. Using these data, we calculate a magnetic component $B_p$ which lies in the $(x, y)$ plane and is both perpendicular to the $z$ axis (see Figure 1) and to the direction of the electric antenna. The phase shift between $B_p$ and the electric component gives the sign of the $k_z$ component. A phase difference near to 0° means the waves propagate with $k_z > 0$ (downgoing waves), a 180° phase shift should be obtained for upgoing waves with $k_z < 0$. See appendix for a detailed description of this procedure.

## 3. Characteristics of the Different Emissions

The analysis described in the previous section has been applied to the data of the Freja wave experiment. The sampling frequency in the LF range allows the spectral analysis up to 2 kHz; however, to discuss the ELF waves around $f_{\mathrm{H}+}$ ($f_{\mathrm{H}+}$ is about 400 Hz at Freja altitudes) we have chosen a restricted frequency interval 0–1000 Hz. We present the results based on the measurement during three selected passes.

### 3.1. March 22, 1994

On March 22, 1994, between 1442 and 1508 UT, the satellite passes at an altitude of 1700 km in the morning sector, from auroral to middle latitudes of the northern hemisphere. Magnetic local time (MLT) changes from 0300 to 0900. Corrected geomagnetic latitude (CGLat) decreases from about 65° to 40°. Time-frequency plots of different wave parameters are collected in Plates 1 and 1. During the pass, the evolution of the local $f_{\mathrm{H}+}$ is calculated using the DC magnetic field data. It is plotted by a black line over each of panels. The power spectrograms of the magnetic component $B_z$ (parallel to $\mathbf{B}_0$) and the electric component are presented in Plates 1a and 1b. The electric spectrogram (Plate 1b) is modulated by a regular time-dependent pattern due to the spinning antenna (the basic period of 48 s is given by the interference of the 6-s period of the satellite spin with the 16-s period of data snapshots). The regular red stripes are due to instrumental effects in the electric data, and the absence of the signal in both spectrograms near 1457 UT is due to a data gap.

During the pass, we can observe several types of emissions with different spectral characteristics. The broadband low-frequency noise (denoted as "type D" in section 1) is observed mainly between 1445 and 1447 UT, i.e., at geomagnetic latitude of 65°. The emission is seen in the electric field data, but the spectrograms of magnetic components perpendicular to $\mathbf{B}_0$ ($B_x$ and $B_y$ – not shown) reveal also this low-frequency noise. A hiss emission gradually starts after 1445 UT and remains till the end of the pass. Before 1500 UT, i.e., at latitudes above 55°, the hiss has a sharp lower cutoff at a frequency which is by about 20 Hz below $f_{\mathrm{H}+}$. The spectral characteristics of this emission correspond to the "type A". After 1500 UT, at CGLat $< 55°$, the main cutoff goes down to about 80 Hz below $f_{\mathrm{H}+}$ and another faint band appears in the frequency interval of about 80 Hz below the main cutoff. The upper limitation of the main hiss band is at about 600 Hz. These spectral characteristics well reflect the properties of the "type F" emissions. Finally, waves below $f_{\mathrm{H}+}$ are recorded between 1447 and 1457 UT. The lower-frequency limitation fluctuates from 0.3 $f_{\mathrm{H}+}$ to 0.7 $f_{\mathrm{H}+}$ and there is no stop-band above the emission. The spectral "type C" fits well this description.

Plate 1c shows the ellipticity of the wave polarization. From this plot, we can get information for a given frequency and time, similarly as in the spectrograms. The ellipticity is coded in a color scale between blue (linear polarization) and red (circular polarization). White represents the regions of low signal intensity where the magnetic power-spectral density in Plate 1a is lower than $10^{-8}$ nT$^2$/Hz. This presentation allows to simply compare the parameters of the different types of emissions, as recognized previously in the power spectrograms. We clearly see that the type D low-frequency emissions are linearly polarized. This fact has important consequences for further analysis, as it will be shown later on. The behaviour of the type A waves is more complex. Above $f_{\mathrm{H}+}$, the ellipticity is high and ranges from 0.7 to 1. In the narrow band between $f_{\mathrm{H}+}$ and the lower cutoff, the ellipticity abruptly decreases. The type C waves below the hiss cutoff again have a nearly circular polarization. The ellipticity of the type F emission is around 0.5 at higher frequencies and decreases to a weakly elliptic polarization near the main cutoff. The faint wave band at lower frequencies has again ellipticities of 0.5 – 0.7. Information about the wave polarization is extended in Plate 1d. The sense of polarization in the plane perpendicular to $\mathbf{B}_0$ is indicated by red or green spots. The sense of polarization is obviously undefined when the polarization is linear. Random errors of the spectral analysis cause large uncertainties of the polarization sense also for a weakly elliptical polarization. Regions where the ellipticity is lower than 0.2 are thus whitened (this concerns mainly the type D waves), in addition to regions where the signal intensity is lower than $10^{-8}$ nT$^2$/Hz. The type A emission is right-hand-polarized above $f_{\mathrm{H}+}$. In the narrow band between the cutoff and $f_{\mathrm{H}+}$ left polarized waves sometimes emerge mainly between 1457 and 1500 UT. The type C emission is circularly right-hand-polarized. The type F waves conserve the right-hand polarization, even several tens of hertz below $f_{\mathrm{H}+}$. The left-hand-polarized waves appear just at the lower edge of the faint band, especially between 1500 and 1503 UT.

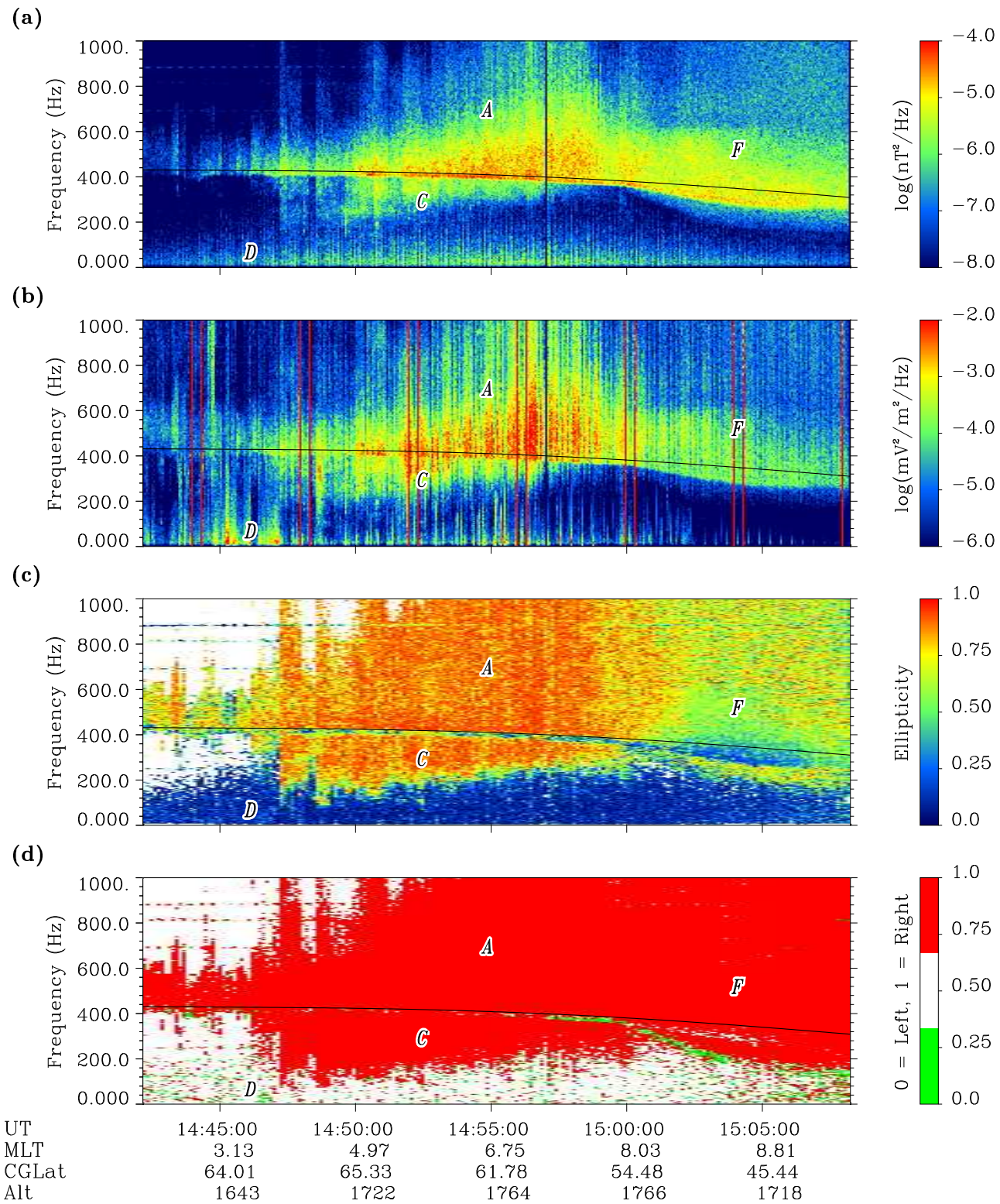


**Plate 1.** Wave parameters on March 22, 1994: (a) spectral power density of the magnetic $B_z$ component; (b) spectral power density of the electric component measured by a spinning antenna; (c) ellipticity (a value of 1 means circular polarization); (d) sense of elliptic polarization (green corresponds to the left-hand polarization; red means the right-hand sense). The local $f_{H+}$ is plotted by a black line, and the different spectral types are indicated by letters (see text).

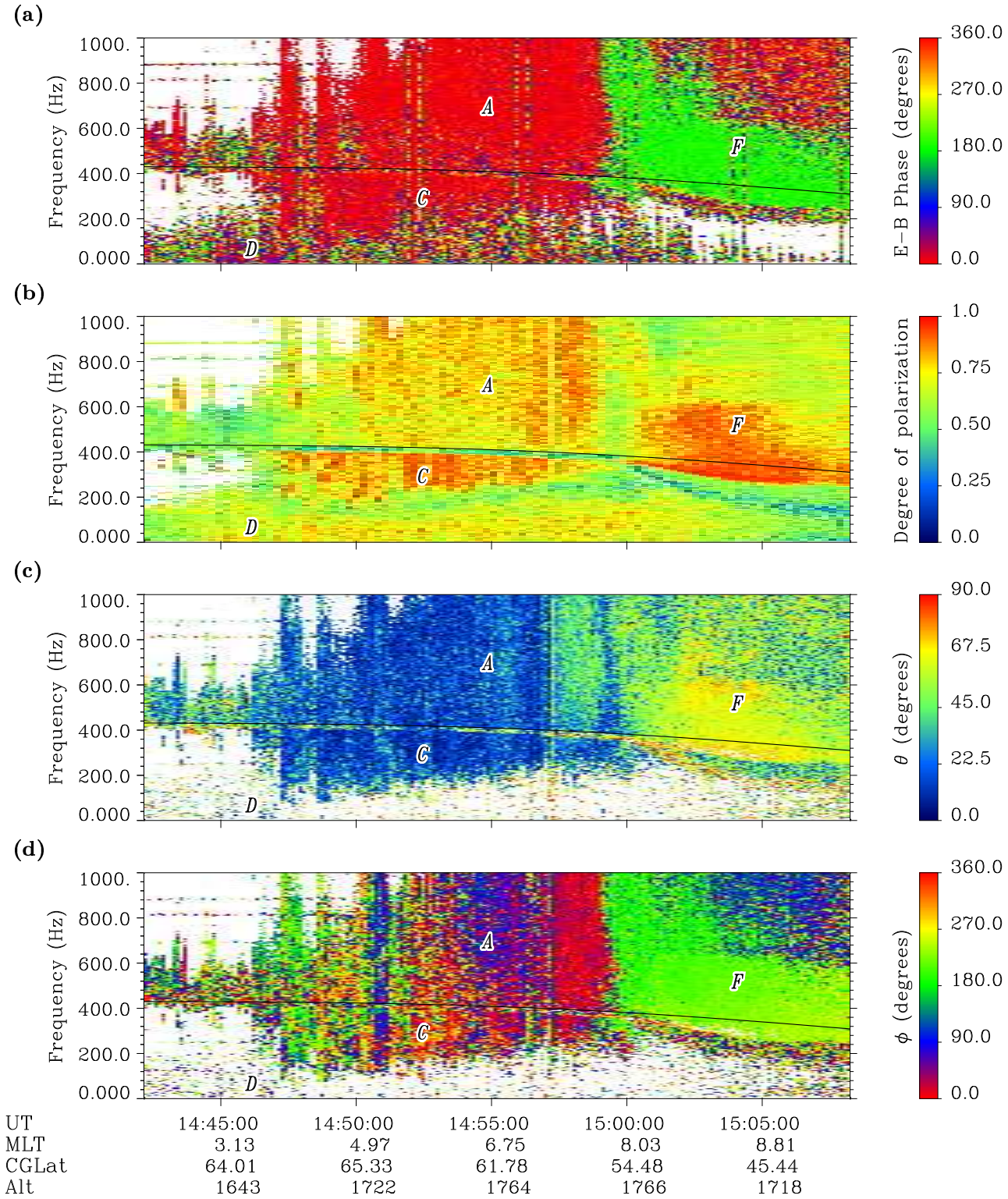


**Plate 2.** Wave parameters on March 22, 1994 (continued): (a) phase shift between the electric $E_a$ and the magnetic $B_p$ components indicating the downward (red) or upward (green) propagation; (b) degree of polarization (a value of 1 corresponds to the presence of a single plane wave); (c) angle $\theta$ defining the deviation of the wave vector from $\mathbf{B}_0$; (d) angle $\phi$ giving the azimuth of the wave vector, $\phi$=0° is in the direction of decreasing CGLat for downward propagation. The local $f_{\mathrm{H}+}$ is plotted by a black line, and the different spectral types are indicated by letters (see text).

The observed features of the wave polarization are obviously connected to the properties of the wave propagation in the plasma medium. Several propagation parameters are presented in Plate 1. In Plate 1a we can see whether the waves go down or up with respect to the $\mathbf{B}_0$ direction. As expected, the phase between the electric and the magnetic $B_p$ components is near either 0° or 180° (see appendix). The red regions in this panel therefore correspond to waves propagating toward the Earth and the green regions to upgoing waves. The regions of low signal intensity are whitened (the magnetic spectral density lower than $10^{-8}$ nT$^2$/Hz and the electric spectral density lower than $10^{-6}$ mV$^2$/m$^2$/Hz). We observe that the type A and type C emissions between 1447 and 1459 UT are clearly downgoing. The low-frequency type D emission is probably downgoing, but the interpretation is much less reliable than in the previous case, because of large fluctuations in both frequency and time domains. On the other hand, the type F emission above the main cutoff is clearly upgoing. Oppositely, the faint waves below this cutoff seem to propagate rather downward.

A measure of the wave field complexity is given by the degree of polarization presented in Plate 1b. Again, the regions where the magnetic signal intensity is low are whitened. The type D emissions at low frequencies are generally well polarized, with a polarization degree around 0.8. The same values for the type A hiss above $f_{\mathrm{H}+}$ range between 0.5 and 1. This means that the wave field can be often described by a single plane wave, but sometimes the distribution of wave vector directions could be more complex. In the narrow band between the sharp cutoff and $f_{\mathrm{H}+}$ the polarization degree becomes very low. This may agree with a possible propagation of two cold plasma modes restricted to this band. The low polarization degree could also reflect a complex distribution of wave vector directions including a mixture of downgoing waves with reflected upgoing waves. The simultaneous propagation of both right-hand-polarized and left-hand-polarized waves could also explain the low ellipticity and the sporadic detection of the left-hand polarization noted above. The type C waves have a high polarization degree, which indicates the validity of the plane wave hypothesis. The type F emission propagates as plane waves above the main cutoff. The faint band at lower frequencies is less polarized, and a very low polarization degree at the lower edge of this band is possibly again due to the simultaneous presence of two wave modes, or to an increased complexity of the wave field.

The propagation effects become clearer knowing the full wave vector direction. Obviously, this direction is well defined only if the polarization degree is high enough. Plates 1c and 1d present respectively the two angles $\theta$ and $\phi$ defined in Figure 1. The regions of low signal intensity (lower than $10^{-8}$ nT$^2$/Hz) are again whitened. The method we use is unable to determine these angles if the wave polarization is linear. For weak ellipticities the obtained wave vector direction is strongly influenced by random errors of the spectral analysis. We have therefore used an ellipticity threshold of 0.2, below which the data are whitened, similarly as in Plate 1d. This again concerns mainly the type D emissions where we obtain randomly fluctuating values and where we are not able to determine the wave vector direction. The type A hiss propagates mainly at low $\theta$, i.e., nearly parallel to $\mathbf{B}_0$. This causes large uncertainties and low relevance of $\phi$ determination. The $\theta$ values are larger only in the beginning and in the end of the type A hiss emission. Around 1447–1448 UT, $\phi$ values indicate a propagation toward increasing magnetic latitudes. Before 1500 UT, $\theta$ grows to about 40°, and $\phi$ corresponds to an equatorward propagation (toward decreasing CGLat). The narrow band below $f_{\mathrm{H}+}$ has a low polarization degree and interpretation of obtained $\theta$ and $\phi$ values would be dubious. The type C waves propagate very similarly as the hiss at higher frequencies, but the parallel propagation remains during all the time interval. This propagation direction also corresponds to much higher spectral densities of the perpendicular magnetic components ($B_x$ and $B_y$ – not shown). On the other hand, the type F waves propagate above the main cutoff mainly at high $\theta$ angles around 70°. The corresponding $\phi$ values are about 180°. This again indicates the equatorward propagation since the waves are upgoing. This direction could be consistent with possible low-altitude reflection of the equatorward propagating part of type A hiss. The faint band below the main cutoff seems to propagate nearly parallel to $\mathbf{B}_0$, but the low polarization degree does not allow a reliable interpretation.

### 3.2. June 14, 1993

The next example in Plates 1 and 1 presents a Freja observation on June 14, 1993. Unlike the previous case, the satellite passes in the evening sector at MLT between 1700 and 2200 and at CGLat increasing from 45° to 73°. All panels are similar as in Plates 1 and 1, including the threshold values of unreliable data which again appear as white regions. Note that the overall level of wave intensity is lower than in the previous case. The spectrograms reveal several types of emissions. First, the type F hiss appears at lower latitudes. Its blurred lower-frequency limit extends down to about 100 Hz below $f_{\mathrm{H}+}$. Around 640 Hz we note a distinct stop band in both electric and magnetic spectrograms. As shown in other panels of Plates 1 and 1, the main part of the emission below and above the stop band consists of right-hand elliptically polarized and nearly plane waves. They propagate upward in the direction of decreasing CGLat. The angle deviation from $\mathbf{B}_0$ gradually decreases: as the satellite passes to higher latitudes the propagation direction changes from nearly perpendicular to oblique (Plate 1c). The faint waves inside the stop-band seem to propagate downward at low $\theta$ but their polarization degree is lower.

After 0340 UT, the stop band disappears and the spectral shape of the hiss change to the type A emission with a sharp lower cutoff. In the narrow band between the cutoff and $f_{\mathrm{H}+}$, the low ellipticity and polarization degree could be attributed to the presence of both cold plasma modes or a complex wave vector distribution. Above $f_{\mathrm{H}+}$ the waves are right polarized and mainly downgoing. Between 0340 and 0344 UT, we note a gradual decrease of $\theta$ and an equatorward propagation for frequencies above about 500 Hz. These properties and a high polarization degree resemble the evolution of the type F emission at lower latitudes, especially above the stop-band. The reflection of the type A hiss below the spacecraft trajectory may possibly explain the observations. A short interval of a lower polarization degree observed at all frequencies between 0339 and 0340 UT could then correspond to the presence of both downgoing and reflected upgoing waves. This may also be the case of the type A hiss below 500 Hz. After 0345 UT (at latitudes above 65°), the hiss propagates poleward at low $\theta$. For CGLat $> 70°$, the waves are limited in a band of about 200 Hz above $f_{\mathrm{H}+}$ and the upgoing propagation becomes significant. This could again be explained by the reflection at lower altitudes.

During all the pass we can identify the low frequency type D noise. The intensity is increasing just before 0339 UT and then after 0345 UT till the end of the record. The waves are strictly linearly polarized with a high polarization degree and a probable downward propagation. Between 0345 and 0346 UT we observe a distinct type C emission. In the power spectrograms, the lower-frequency limit is hidden by the type D noise. However, other panels show a clear circularly right-hand-polarized emission of downgoing field-aligned waves propagating between about 80 and 400 Hz. An interesting feature can be noted between 0343 and 0345 UT, just before the main type C emission. In the magnetic spectrogram we can see a pair of faint oblique stripes. Their frequency increases from 100 to about 350 Hz. The detailed analysis shows that the stripes consist

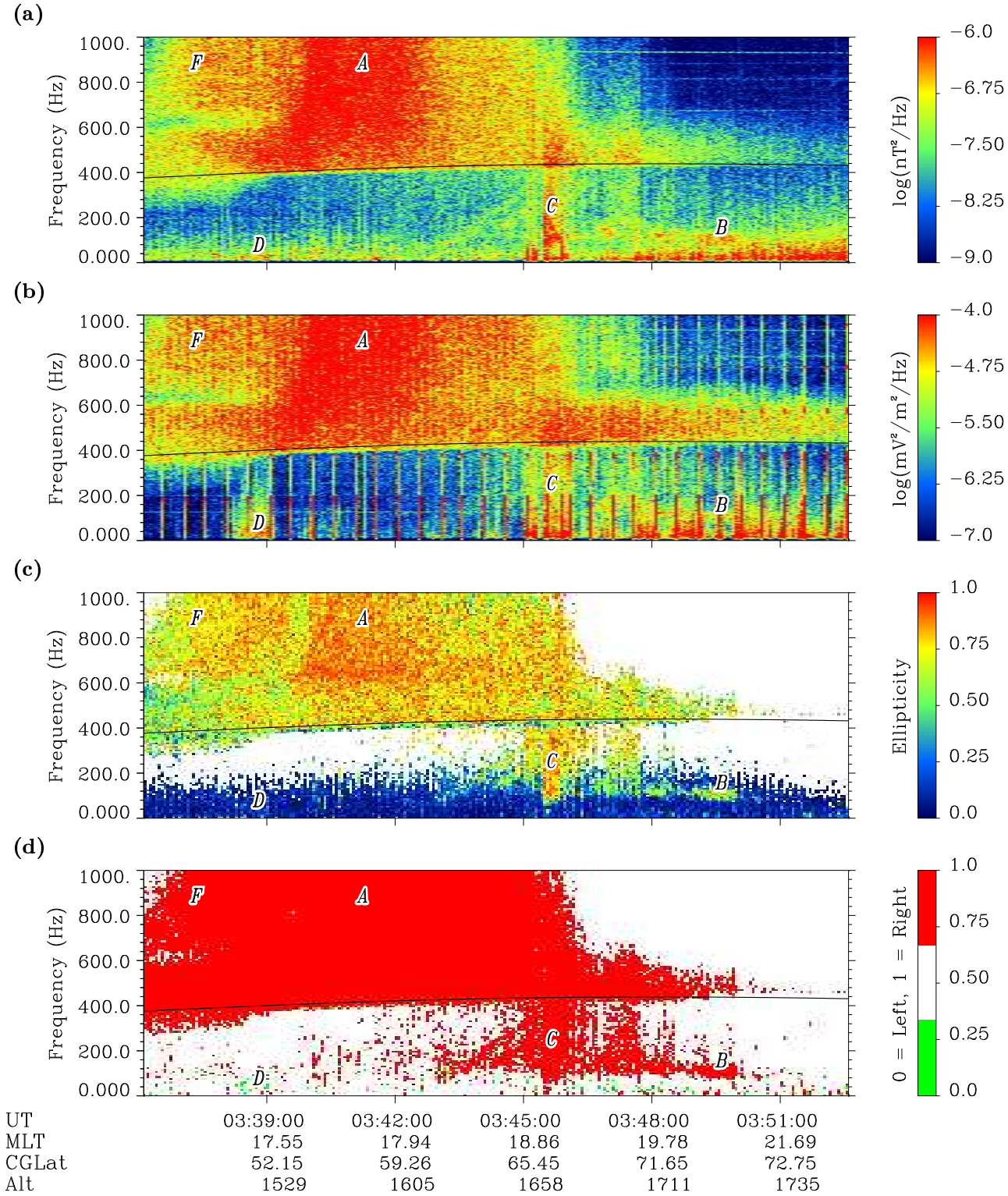


**Plate 3.** Wave parameters on June 14, 1993: The same parameters as in Plate 1 with an exception that Plate 1a presents the spectral power density of the magnetic $B_y$ component.

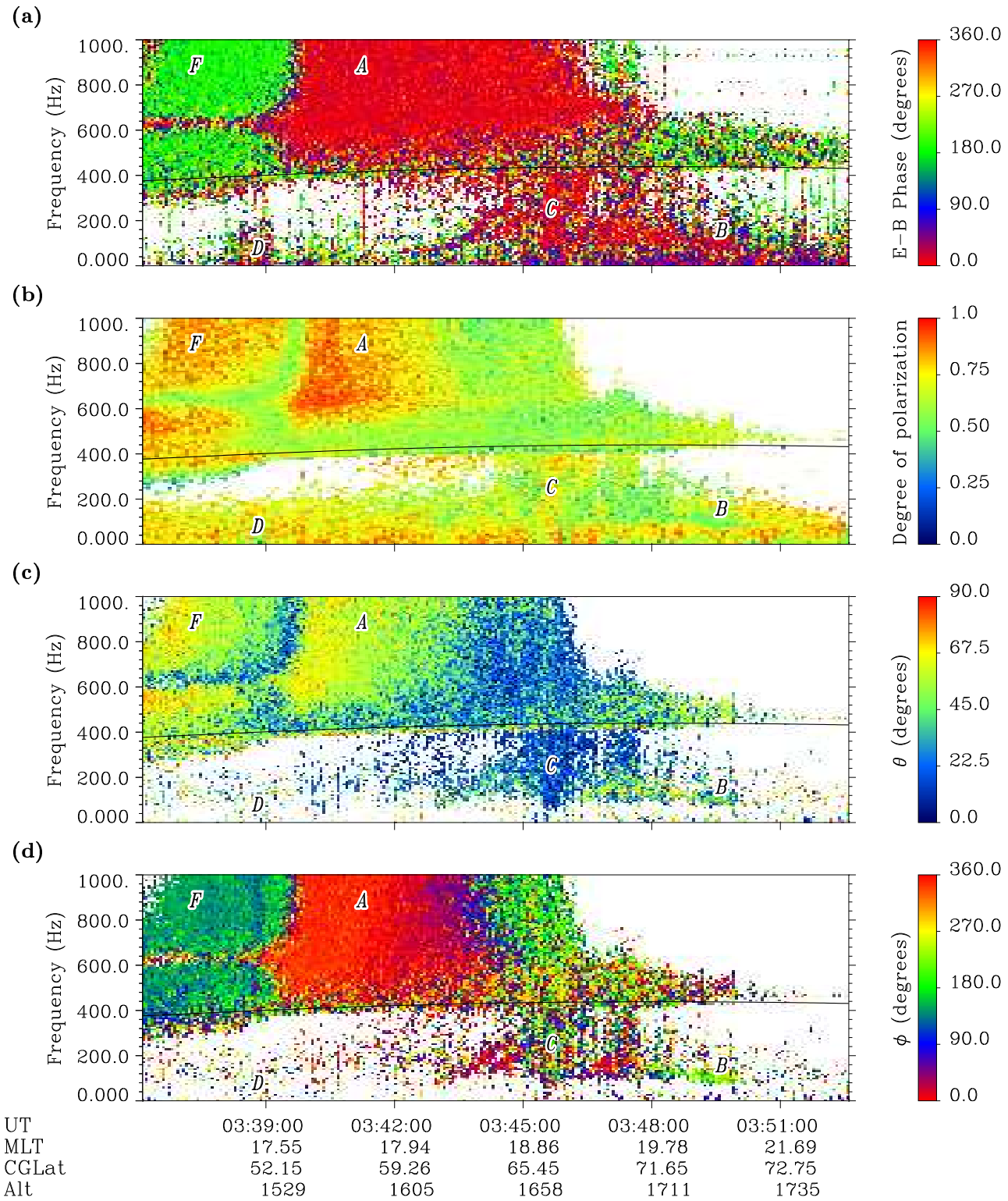


**Plate 4.** Wave parameters on June 14, 1993 (continued): The same parameters as in Plate 1.

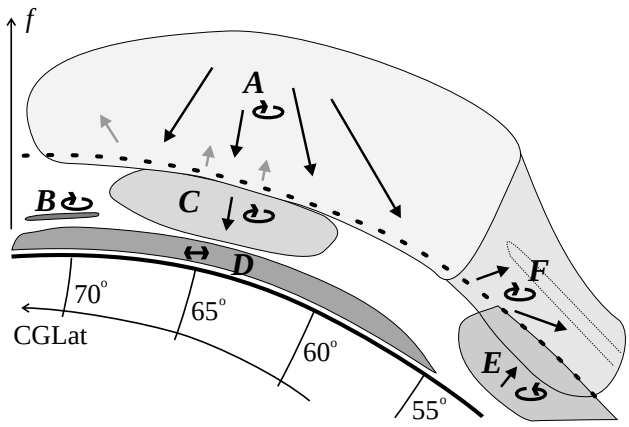


**Figure 2.** Basic polarization and propagation characteristics of six different types of electromagnetic emissions.

of elliptically right-hand-polarized waves propagating downward to the equator with $\theta$ decreasing from about 40° to a few degrees. Narrowband waves at about 100 Hz can be identified between 0347 and 0350 UT, mainly in the magnetic field spectrogram. Although the emission is partly disturbed by the type D noise, it can be categorized as type B waves. Further analysis reveals right-hand elliptically polarized waves emerging from the noise of linear polarization. Consistently with the widely accepted generation model involving the auroral electron beams [*Temerin and Lysak*, 1984], the waves propagate downward. However, the expected quasi-perpendicular propagation is not confirmed by the present analysis. The $\theta$ values seem to be below 50° with a probably northward azimuth between 0349 and 0350 UT. On the other hand, the polarization degree is rather low (probably due to the simultaneous presence of the type D noise) and the obtained $\mathbf{k}$ direction has a low reliability.

### 3.3. June 23, 1993

The third example has been recorded on June 23, 1993 (Plates 2 and 2). The data handling is again similar as in previous Plates. The spacecraft passes from the evening to the night sector at altitudes between about 1700 and 1550 km. The magnetic latitudes first grow from about 60° up to 68°, and then decrease down to about 46°. An equatorward propagating type A hiss is seen in the beginning of the pass. The emission manifests some features discussed already in the previous two examples, including a possible mixture of upgoing and downgoing waves above $f_{\mathrm{H}+}$, and complex two-mode and/or propagation phenomena in a narrow band between the sharp lower cutoff and $f_{\mathrm{H}+}$. Simultaneously, right-hand-polarized type C waves propagate downward, in a nearly field-aligned ($\theta$ <30°) and slightly equatorward direction. The lower-frequency limitation of this emission is at about 80 Hz. Below this frequency we note a linearly polarized type D noise. This spectral type persists during nearly all the pass and the electric field signatures extend occasionally up to several hundreds of hertz (e.g., between 0555 and 0559 UT).

In the second half of the pass, the overall appearance of the power spectrograms becomes nearly inverse. After 0600 UT, we observe an emission with an upper limit exactly at $f_{\mathrm{H}+}$ and also another faint band just below the local helium gyrofrequency $f_{\mathrm{He}+}$. These features of type E waves are distinctly seen only in the magnetic spectrograms. The emissions below $f_{\mathrm{H}+}$ are accompanied by a bursty emission above $f_{\mathrm{H}+}$. Further analysis reveals the type E waves below $f_{\mathrm{H}+}$ and below $f_{\mathrm{He}+}$ are clearly upgoing. The same holds true for the waves above $f_{\mathrm{H}+}$. The emissions around $f_{\mathrm{H}+}$ manifest a high degree of a nearly circular polarization, whereas in the faint emission below $f_{\mathrm{He}+}$ the polarization degree is low, probably due to simultaneous presence of the linearly polarized magnetic turbulence. The polarization sense is left handed inside the emissions below $f_{\mathrm{He}+}$ and $f_{\mathrm{H}+}$, and right handed elsewhere. Estimates of $\theta$ and $\phi$ angles show that the right-hand-polarized parts of the emission propagate equatorward mainly at low angle deviations from $\mathbf{B}_0$ ($\theta$ <45°). Similar analysis for the left-handed waves gives $\theta$ near 0° and therefore highly fluctuating $\phi$ values.

## 4. Discussion

A simple sketch in Figure 2 attempts to summarize basic features of the different emissions shown in Plates 1–2. First, Figure 2 can be read as a simplified spectrogram, assuming that the satellite passes over an imaginary local meridian from higher to lower magnetic latitudes. The thick solid line above the CGLat labels represents the zero frequency, and the thick dotted line means $f_{\mathrm{H}+}$. Each group of emissions is indicated by a shaded area with a letter defining the emission type, and a pictogram symbolizing the wave polarization. Second, Figure 2 can be read as a sketch of the satellite trajectory over the same imaginary local meridian. The thick solid line then represents the Earth's surface and the satellite moves along the thick dotted line. In this case, arrows stand for wave vector directions of a given emission type at a given CGLat, assuming the propagation in the plane of the local meridian. Note that this second meaning provides only schematic information about the propagation directions at the altitude of the satellite orbit. It should not be confused with an altitude-dependent plot.

### 4.1. Type A

The downgoing low-altitude type A hiss is observed on subauroral and auroral latitudes between 55° and 70°. A sharp lower cutoff just below $f_{\mathrm{H}+}$ is a dominant feature of these emissions. A generally accepted explanation of this cutoff has been first proposed by *Gurnett and Burns* [1968]. The downpropagating waves penetrate the magnetized multi-ion plasma with growing $f_{\mathrm{H}+}$ and a decreasing hydrogen fraction. The waves encounter growing multi-ion frequencies below $f_{\mathrm{H}+}$ and the originally right-hand-polarized obliquely propagating hiss changes the polarization sense at the multi-ion cross-over frequency $f_{\mathrm{co}}$. The resulting left-hand-polarized wave is then cut off at the multi-ion cutoff frequency $f_{\mathrm{cL}}$ [*Smith and Brice*, 1964]. As it follows from this scenario, the cutoff is produced at the place of observation. It should be therefore very sharp and coherent with the local characteristic frequencies. Returning to the spectrograms in Plate 1, we observe that before 1500 UT, in the region of downgoing type A waves, the cutoff below $f_{\mathrm{H}+}$ is very sharp. According to the theory of multicomponent cold plasmas [*Smith and Brice*, 1964], the location of the observed cutoff at $f_{\mathrm{cL}}$ implies ion composition with 5% of $\mathrm{H}^+$ and 95% of $\mathrm{O}^+$, supposing a simple model of a single ionized hydrogen-oxygen plasma. This ion composition is well consistent with estimates of the local lower hybrid and plasma frequencies. The lower hybrid frequency ($f_{\mathrm{lh}} \approx 3$ kHz) has been identified with the lower cutoff of the electrostatic (and therefore local) hiss emissions found in the MF range of the Freja wave experiment. The local plasma frequency $f_{\mathrm{p}}$ is obtained from the electron density measured by Langmuir probes of the wave experiment and also from spontaneous emissions of Langmuir waves recorded around 450 kHz in HF range of the wave experiment. The consistency with the local plasma parameters therefore suggests that the cutoff of the type A emission is well coherent with the above scenario.

The type A emissions are right-hand circularly polarized except a narrow frequency band between the sharp cutoff and $f_{\mathrm{H}+}$ where

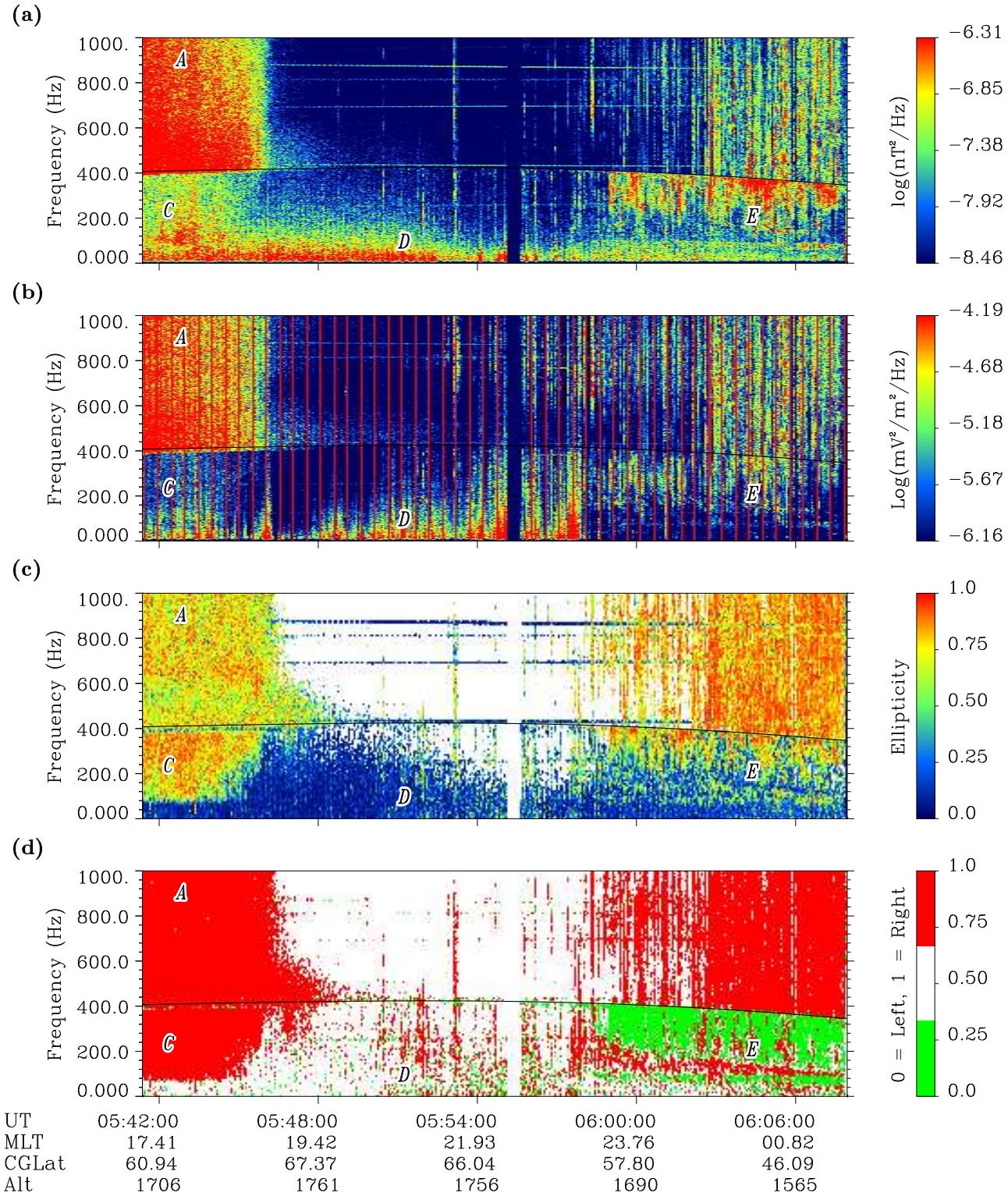


**Plate 5.** Wave parameters on June 23, 1993: The same parameters as in Plate 1 with an exception that Plate 2a presents the spectral power density of the magnetic $B_x$ component.

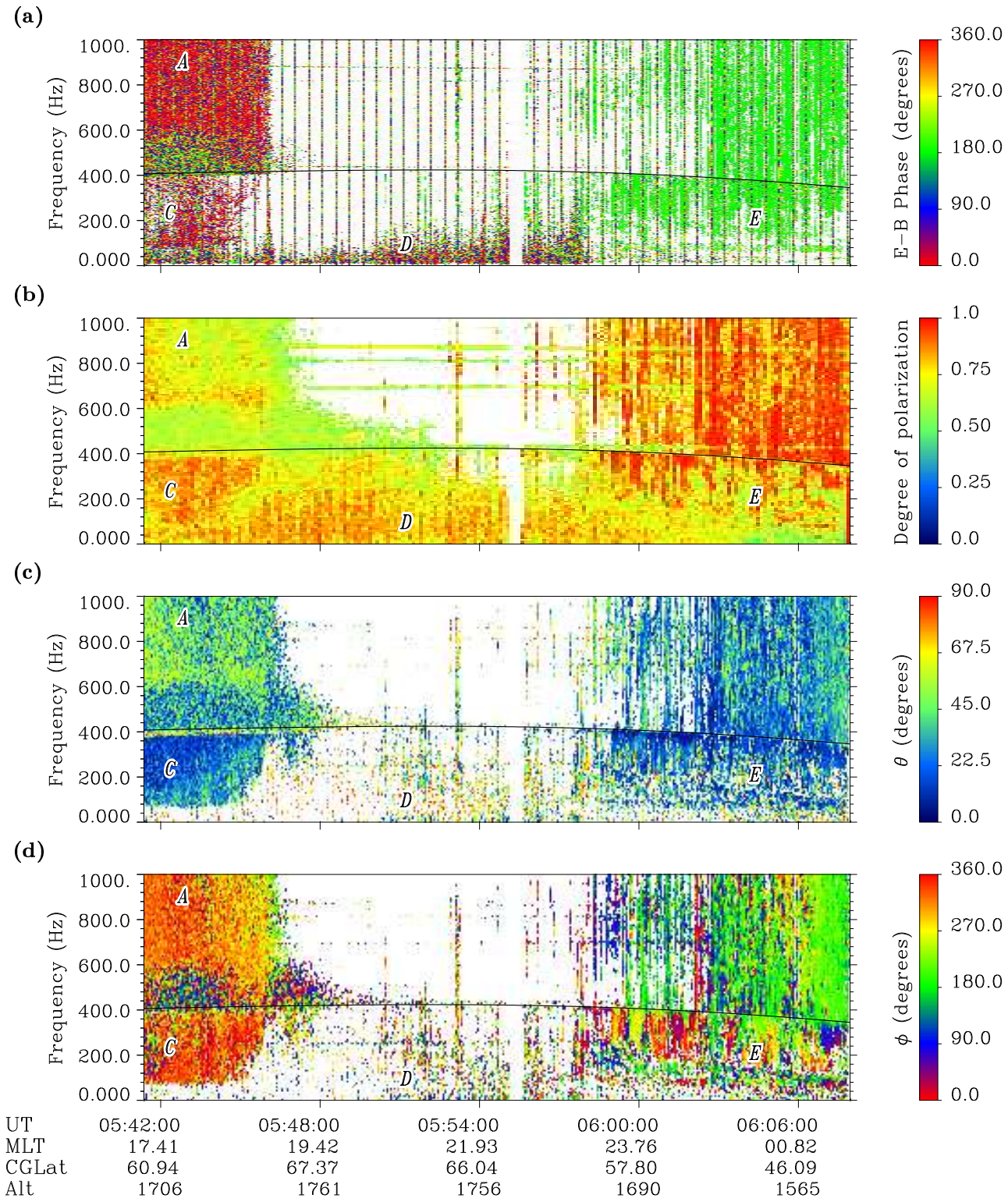


**Plate 6.** Wave parameters on June 23, 1993 (continued): The same parameters as in Plate 1.

we probably observe a mixture with left polarized and/or reflected waves. Similar narrow band of left-hand-polarized waves just below $f_{\mathrm{H}+}$ as obtained in Plate 1 has been found by *Lefeuvre et al.* [1992] and *Rauch et al.* [1993] in the Aureol 3 data. A mixture of downgoing and reflected waves could be present also above $f_{\mathrm{H}+}$ as shown, e.g., in Plate 2. This confirms the Aureol 3 observations [*Lefeuvre et al.*, 1992]. The type A hiss is often nearly field-aligned, but we observe signatures of a divergence of propagation directions at both latitudinal edges of the emission: the equatorward propagation at lower latitudes and the poleward propagation at higher latitudes. An upgoing band-limited hiss is sometimes observed on the poleward edge of the emissions. This last feature has not been noted in the Aureol 3 data, and can be explained by the reflection of the poleward propagating part of the type A emissions, probably at the two-ion cutoff frequency $f_{\mathrm{cL}}$. This reflection mechanism can explain the limitation to a band of about 200 Hz above $f_{\mathrm{H}+}$ (see the discussion of the type F emissions). A statistical study would be necessary to check these signatures. Our case study indicates that the hiss comes from higher altitudes outside the plasmasphere, consistently with the conclusions given by *Lefeuvre et al.* [1992]. However, the examination of the generation mechanism is beyond the scope of this paper.

### 4.2. Type B

The type B narrow band emissions are often hidden in the low-frequency turbulence at Freja altitudes. Our analysis gives the right-handed elliptic polarization and downward propagation. It also indicates rather low $\theta$ values, but the results are not sufficiently reliable because of a possible interference with the type D noise. If the propagation at lower $\theta$ is confirmed, we need to take into account additional propagation effects to reach the consistence with the generation model based on beams of auroral electrons [*Temerin and Lysak*, 1984]. In a recent case study of a similar emission, *Oscarsson et al.* [1997] found a much better consistence with the traditional generation mechanism.

### 4.3. Type C

The type C emissions below $f_{\mathrm{H}+}$ manifest a highly elliptic right-handed polarization and a nearly field-aligned downward propagation, in all the cases we have presented. The same properties have been previously found in two Aureol 3 case studies [*Rauch et al.*, 1985; *Lefeuvre et al.*, 1992]. A statistical analysis also confirms these results [*Santolík and Parrot*, 1998]. The statistics further show that the emissions occur mainly at magnetic latitudes above 60° on the dayside, and that the estimates of the phase velocity roughly agree with the cold plasma theory. A sharp cutoff between 0.1 and 0.4 $f_{\mathrm{H}+}$ is sometimes observed, but more frequently the spectra reveal a diffuse or fluctuating lower frequency limit. *Rauch et al.* [1985] proposed three kinds of possible generation mechanisms. First, the waves can be generated at low altitude above the satellite by energetic protons. Second, the waves can be emitted by a similar mechanism as proposed by *Temerin and Lysak* [1984], and experience subsequently a polarization reversal and/or a refraction to low $\theta$ values. Third, a part of a nearly field aligned type A hiss can penetrate below the two-ion crossover frequency $f_{\mathrm{co}}$ during the downward propagation, and stay in the right-hand-polarized mode. Contrary to the conclusions of *Rauch et al.* [1985], we believe that the last hypothesis could be the most promising. The theory on the waves just below $f_{\mathrm{H}+}$ in an inhomogeneous dipole magnetic field [*Le Quéau et al.*, 1993; *Chust and Le Quéau*, 1996] indicates a possibility of the hiss tunnelling below $f_{\mathrm{co}}$ in some finite range of nonzero $\theta$ values. However, reliable conclusions cannot be done without further quantitative modelling of this process.

In Plates 1 and 1, we have shown an emission consisting of a pair of faint stripes with increasing frequency, located equatorward from the regular type C emission. We have found five more similar phenomena in our data set. Some of them have a spectral form of a gradually growing upper cutoff of a faint emission, but the overall properties are always similar. All these "frequency drift phenomena" are observed at similar frequencies and at latitudes between 59° and 68° in the afternoon or evening sector. The frequency increases by 200–330 Hz during 80–150 s. Estimates of a possible spatial frequency drift are of the order of 50–130 Hz per degree of magnetic latitude. The starting frequency lies between 80 and 150 Hz and is essentially the same as the lower limitation of the subsequent type C emission. As far as we know, no similar satellite observations has been previously reported in this frequency range. Some similarities can be however found in ground based observations of *Heacock* [1974]. The geomagnetic latitude of these measurements (65°), the frequency range (20–200 Hz, peak occurrences at 80–90 Hz), the absolute value of the slope and the duration (60–100 Hz during 15–90 s) are roughly similar to our observations. The prevailing dayside occurrences agree with the statistics of occurrences of the type C emissions [*Santolík and Parrot*, 1998]. The events occurring simultaneously at different frequencies (15% of the total cases of *Heacock* [1974]) could be similar to the "double stripe" feature in Plates 1 and 1. The main difference is that nearly all events of *Heacock* [1974] fall in frequency with time, whereas our events rise in frequency. The spectral shape of these phenomena is probably connected to their generation mechanism. Let us suppose their origin is the same as the generation mechanism of the associated type C waves, and assume the hypothesis about the tunnelling of the type A emissions below $f_{\mathrm{co}}$. Then, these faint emissions could provide an indication about the origin of the type A hiss, which is still an open question.

### 4.4. Type D

The type D low-frequency noise has generally a high degree of a nearly linear polarization. The data sometimes seem to indicate a downward propagation, but no reliable conclusion about the wave propagation can be made. We possibly include several kinds of turbulence into the same spectral type. However, the explanation by means of solitary kinetic Alfvén waves [*Wahlund et al.*, 1994] and/or Alfvén resonance cavities [*Stasiewicz et al.*, 1997] could be consistent with the observations. The noise could occur at low frequencies due to the Doppler shift induced by the satellite motion, consistently with the observed linear and high-degree polarization.

### 4.5. Type E

Plates 2 and 2 show plasmaspheric type E emissions with a sharp upper cutoff. We have observed similar properties of upgoing and left-hand-polarized type E emissions in several other passes, all of them on the nightside (at MLT from about 2030 to 0300), and inside the plasmasphere (at CGLat below about 55° which corresponds to $L$ parameter below 3.5 at Freja altitudes). The upward propagation well explains the observed sharp limitation of wave spectra at $f_{\mathrm{H}+}$ and $f_{\mathrm{He}+}$. Upgoing waves penetrate the medium with decreasing magnetic field strength and the left-hand-polarized waves come into the resonance at the gradually decreasing local ion gyrofrequency. This leads to the dissipation of wave energy into the plasma, and waves at the resonant frequency are absorbed and removed from the frequency spectra which was probably much broader at lower altitudes. The sharp upper frequency limit is always located exactly at the local ion gyrofrequencies.

All these properties strongly resemble to those of the ion cyclotron whistlers first described by *Gurnett et al.* [1965]. The "emissions" below $f_{\mathrm{H}+}$ and $f_{\mathrm{He}+}$ then would correspond to proton and

helium whistlers respectively. The associated right-hand-polarized "emissions" could be therefore attributed to electron whistlers. The typical duration of proton whistlers of *Gurnett et al.* [1965] is between 1 and 4 s. Thus we cannot see their characteristic traces in the time scale of Plates 2 and 2. The data record is not suitable for a more detailed classical analysis in this case (the waveforms are taken in snapshots of only 0.375 s repeated each 2 s). To analyze these short waveform records, we have used the procedure of *Lagoutte et al.* [1992] which is based on the wavelet transform. The method allows to obtain time-frequency plots of wavelet coefficients. These plots are similar to the power spectrograms but have an enhanced temporal resolution at higher frequencies. Plate 2 shows the results. A single data snapshot recorded in the beginning of the type E wave activity has been processed. The bottom part of Plate 2 gives similar information as the classical power spectrograms. Four ion whistler traces can be recognized, starting at offsets of about 50, 120, 200, and 300 ms. Their frequency grows from about 200 Hz and continues to approach the local $f_{\mathrm{H}+}$. Following *Gurnett et al.* [1965], the lower-frequency limit can be interpreted as the multi-ion cross-over frequency $f_{\mathrm{co}}$. At $f_{\mathrm{co}}$ the proton whistlers are coupled with the associated electron whistlers. The electron whistlers have opposite slope in the time-frequency plane and could be detected mainly at higher frequencies. The above interpretation is further supported by the top panel of Plate 2. The wavelet analysis of the mutual phase between the magnetic $B_x$ and $B_y$ components allows us to recognize left-hand-polarized and right-hand-polarized waves. It is clearly seen that the phase shift is about 270° in the proton whistler traces, and thus the waves are left-hand-polarized. On the other hand, the corresponding electron whistlers contain the right-hand-polarized waves with a phase shift of 90°. The detailed analysis presented in Plate 2 proves that the type E "emission" is composed of a large number of discrete ion whistlers.

### 4.6. Type F

Elliptically right-hand-polarized type F emissions are detected equatorward from the type A hiss. The waves are upgoing and propagate at highly oblique $\theta$ (50° – 70°) toward lower magnetic latitudes, which is in agreement with observations of *Mosier* [1971] and *Lefeuvre et al.* [1992]. Returning again to Plate 1, we observe a sharp lower cutoff after 1500 UT, similarly to the type A emission. However, the main part of the type F hiss propagates upward and the above mentioned explanation of *Gurnett and Burns* [1968] becomes invalid. It is probable that the main cutoff of this emission does not have a local origin. Its existence may be explained by a previous propagation through a distant plasma medium with about 20% of $\mathrm{H}^+$, supposing a similar $f_{\mathrm{H}+}$ value as at the place of observation. On the other hand, the low-intensity waves below the main cutoff propagate downward and could have a local cutoff at $f_{\mathrm{cL}}$. The lower limitation of this band corresponds to $f_{\mathrm{cL}}$ if we suppose a plasma with about 50% of $\mathrm{H}^+$. This composition roughly agrees with $f_{\mathrm{lh}}$ and $f_{\mathrm{p}}$ values estimated from local measurements (see the discussion of the type A hiss). This increased hydrogen contents is naturally explained by the fact that the satellite descended to lower latitudes, escaped the high-latitude "light ion trough" region, and entered the plasmasphere (as supported also by the Langmuir probe data).

*Lefeuvre et al.* [1992] concluded that reflection of the downgoing ELF hiss is a possible source of upgoing waves observed at lower latitudes. Reflection at the two-ion cutoff frequency is mentioned as the main mechanism, but no conclusion is given about the possibility of reflection on the ionospheric $E$ and $D$ layers. However, there is another dominant property of the type F emissions which could give further indications about the reflection mechanisms: the emissions often have an upper limitation at 500–700 Hz, as first described by *Muzzio and Angerami* [1972]. Alternatively, at frequencies of 500–700 Hz a stop band is observed, as presented by *Rauch et al.* [1985] and *Hayakawa et al.* [1985]. We believe the upper limitation of the upgoing type F waves is well consistent with reflection at the two-ion cutoff frequency $f_{\mathrm{cL}}$. This frequency grows with decreasing altitude, mainly due to the increasing Earth's magnetic field. Therefore waves at higher frequencies are reflected at lower altitudes, and in our case waves above 500–700 Hz would be normally reflected at altitudes below about 650 km. However, at these low altitudes the reflection process probably becomes inefficient due to an increased collisional frequency and/or decreased $\mathrm{H}^+$ fraction. Thus no waves above 500–700 Hz are reflected. Another reflection mechanism can occasionally create the second band of upgoing waves at higher frequencies. Probable processes are reflection from the ionospheric layers or propagation effects connected with the plasmapause density gradient [*Mosier*, 1971]. A downward propagating band-limited hiss has been however detected in another case not shown here (July 8, 1993, around 1935 UT). In such a case, the above model cannot be used and another mechanism should be applied. The downward propagation in a limited frequency band can be possibly explained by the effects of propagation from the source region located near the equator and at $L \approx 4$, as originally proposed by *Muzzio and Angerami* [1972]. Further statistical analyses of the hiss propagation and ray tracing studies will be useful to understand the complexity of these phenomena.

## 5. Conclusions

We have presented a case study of the wave polarization and propagation involving several types of electromagnetic ELF emissions observed by the low-orbiting Freja satellite. All obtained parameters have been presented as color-coded plots in the time-frequency plane. We have shown that this data representation allows a good characterization of different types of emissions, which are recognized in the power spectrograms around $f_{\mathrm{H}+}$. We have analyzed the waveforms provided by three orthogonal magnetic antennae and one spinning electric antenna. In the ELF range, similar data have been previously analyzed only from the Aureol 3 measurements. We have used several methods of the multicomponent wave analysis and we have developed a new procedure to recognize the upgoing and downgoing waves with these data. The magnetic field records have been used to estimate the properties of the wave polarization, and both magnetic and electric fields have served to fully determine the wave vector direction. The majority of our analysis supposes the presence of a single plane wave. In spite of this restriction we can give several conclusions concerning the wave emissions around the local proton gyrofrequency:

1. We have reproduced the main propagation properties of ELF hiss emissions (types A and F) found previously with the Aureol 3 data [*Rauch et al.*, 1985; *Hayakawa et al.*, 1985; *Lefeuvre et al.*, 1992; *Rauch et al.*, 1993]. These results suggest the waves come from higher altitudes outside the plasmasphere, and reflect at the two-ion cutoff frequency at the altitude of observation and below. At lower latitudes, the waves diverge toward the equator, and after the reflection propagate equatorward and penetrate the plasmapause density gradient.
2. With the improved data representation this upgoing part of the hiss emission (type F) has been better characterized in the present paper. We propose to explain the observed stop-band or band-limitation by means of reflection at the two-ion cutoff frequency.
3. We have demonstrated the divergence of wave vector directions at both latitudinal edges of the hiss emission (type A) and the reflection of poleward turning waves at the two-ion cutoff frequency. These waves then form an upgoing band-limited hiss at the poleward edge of the main hiss emission.

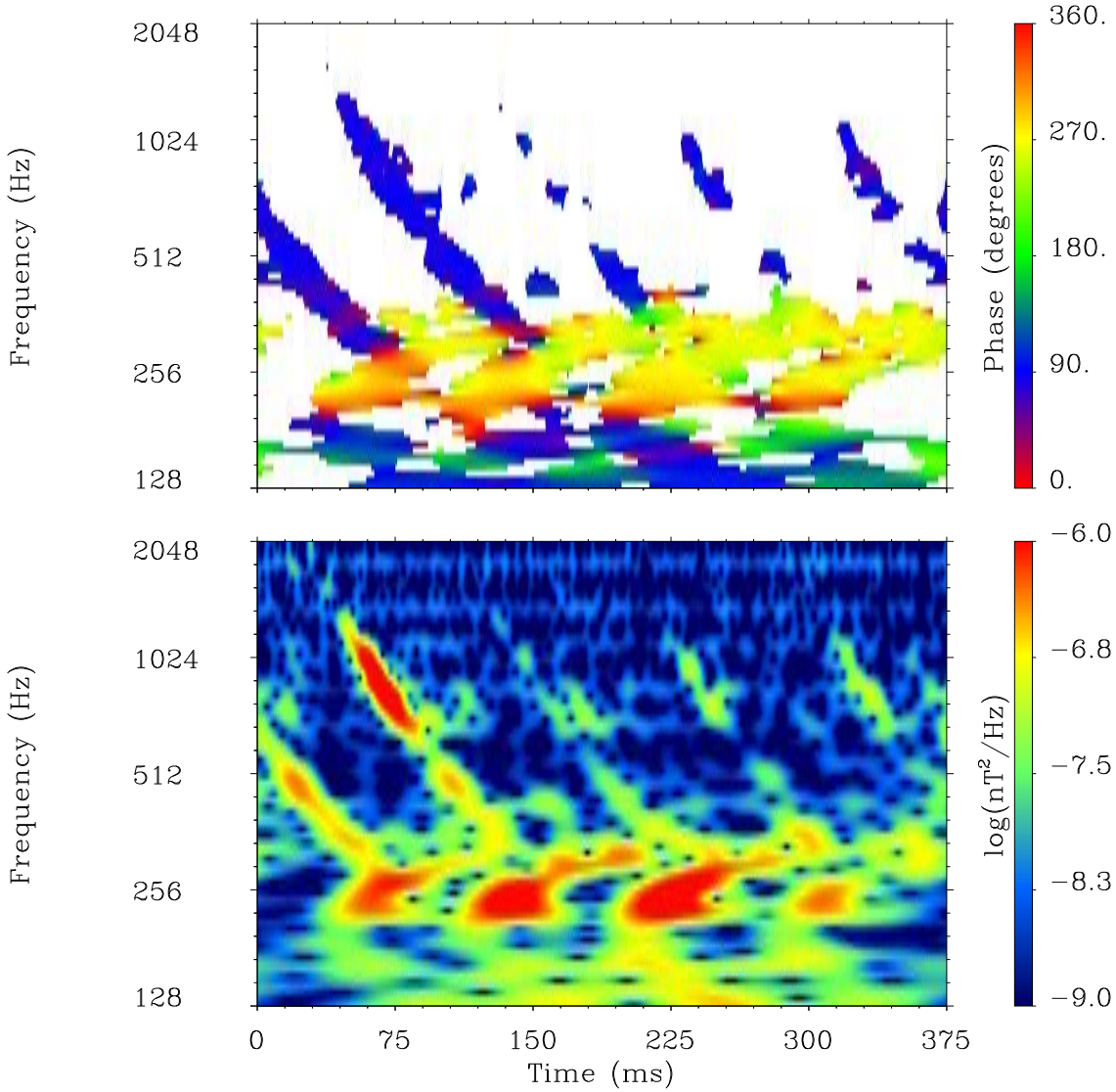


**Plate 7.** Wavelet analysis of a single data snapshot recorded around 0600:03 UT on June 23, 1993. The time scale (horizontal) is given in milliseconds. The frequency scale in hertz (vertical) is logarithmic, and the proton gyrofrequency is about 406 Hz. (bottom) Squared modulus of wavelet coeffi cients calculated for the magnetic $B_x$ component. (top) Phase difference between $B_x$ and $B_y$ obtained by the cross-wavelet analysis.

4. We have confirmed the indications about the broadband auroral emissions below $f_{\mathrm{H}+}$ (type C), given previously in two Aureol 3 case studies [*Rauch et al.*, 1985; *Lefeuvre et al.*, 1992]. We believe that these waves originate from the electromagnetic hiss emissions (type A). The nearly field-aligned downward propagation favors the hypothesis on the tunnelling of right-hand-polarized waves below the two-ion crossover frequency. A statistical study of these emissions is a subject of a parallel paper [*Santolík and Parrot*, 1998].

5. Several cases of faint emissions with "frequency drift phenomena" have been observed equatorward from the regular broadband emissions below $f_{\mathrm{H}+}$ (type C). Probably due to low wave intensity, no similar satellite observations have been reported in the past. Some common features have been found in ground based observations of *Heacock* [1974].

6. The narrow band emissions below $f_{\mathrm{H}+}$ (type B) are right-hand elliptically polarized and propagate downward. The interference with the low-frequency noise does not allow a reliable conclusion about the wave vector direction, but our analysis indicates rather low $\theta$ values.

7. Our results concerning the low-frequency electromagnetic noise (type D) only allow to conclude that these waves are strictly linearly polarized.

8. Plasmaspheric "emissions" with a sharp upper cutoff at the hydrogen gyrofrequency (type E) complete the presented menagerie of electromagnetic waves. The detailed analysis has revealed that they consist of a sequence of upgoing ion whistlers which are repeated as often as once per 100 ms.

Future work, as we hope, will improve the understanding of these several classes of ELF emissions. The low-frequency electromagnetic noise could be better characterized by analysis methods taking into account its linear polarization. Ray tracing and/or statistical studies may help to model the complex of auroral and subauroral wave phenomena that we believe originating in the ELF hiss emissions. Finally, the "frequency drift" cases seem to merit a closer examination which could possibly indicate the generation mechanism also for other types of auroral emissions around the local hydrogen gyrofrequency.

## Appendix: Recognition of Upgoing and Downgoing Waves

With the plane wave hypothesis, recognition of upgoing and downgoing waves is equivalent to the determination of the sign of the wave vector component $k_z$ in the coordinate system of Figure 1. We must use both electric and magnetic data to estimate this sign [*Lefeuvre and Parrot*, 1984]. If the full vector measurement of both fields is available, the problem is reduced to the calculation of the $z$-component of the Poynting vector. However, this is rarely the case and often a lower number of the field components is measured. The electromagnetic mode of the Freja wave experiment provides a three-component magnetic field and a single electric field component measured by a spinning antenna. The methods to reconstruct the wave distribution function, introduced by *Storey and Lefeuvre* [1974, 1979, 1980], can use these data in a natural way to determine the distribution of the energy density in the space of wave-vector directions. When the wave field is near to a single plane wave, the $k_z$ sign can be derived from the obtained distribution. However, the determination of the wave distribution is not always obvious and the procedure is unnecessarily general for the purpose of recognition of upgoing and downgoing waves. Several methods have been published for the Poynting vector measurements using the same number of antennae in the frequency range of Pc1-2 pulsations [*LaBelle and Treumann*, 1992, and references therein]. They are based on the plane wave hypothesis and provide a simple tool for the determination of the $k_z$ sign. They have been generally used for wave frequencies lower or comparable to the satellite spin frequency.

For the Freja data, we have developed a procedure similar to that of *LaBelle and Treumann* [1992]. The difference in our case is that the spin period is much longer than the period of the wave signal. The direction of the electric antenna can be expressed by a unit vector $\hat{\mathbf{a}}$, and an estimate of the measured electric component is

$$E_a = \hat{\mathbf{a}} \cdot \mathbf{E}, \tag{1}$$

where $\mathbf{E}$ is the wave electric field vector. The principal step of this method is the projection of the wave magnetic field to the direction

$$\hat{\mathbf{p}} = \hat{\mathbf{z}} \times \hat{\mathbf{a}}, \tag{2}$$

which lies in the $(x, y)$ plane (Figure 1), and not in the spin plane. This is the difference compared to the method of *LaBelle and Treumann* [1992]. Similar projection is also used in recent Poynting vector calculations based on the Freja data (A. Vaivads et al., Energy transport during $O^+$ energization by ELF waves observed by the Freja satellite, submitted to *Journal of Geophysical Research*, 1998). Following the Faraday's law, theoretical prediction of the wave magnetic field is

$$\mathbf{B} = \frac{1}{\omega}\, \mathbf{k} \times \mathbf{E}, \tag{3}$$

where $\omega$ is the wave angular frequency, and $\mathbf{k}$ is the wave vector. Note that the plane wave hypothesis is used in the above equation. The projection of this vector to the $\hat{\mathbf{p}}$ direction finally reads

$$B_p = \hat{\mathbf{p}} \cdot \mathbf{B} = \frac{1}{\omega}\left(k_z E_a - k_a E_z\right), \tag{4}$$

where $k_a$ is the projection of the wave vector to the direction $\hat{\mathbf{a}}$,

$$k_a = \hat{\mathbf{a}} \cdot \mathbf{k}. \tag{5}$$

From the latter equations it follows that for $E_z = 0$ the phase shift between $B_p$ and $E_a$ is either 0° (for $k_z > 0$) or 180° (for $k_z < 0$), independently of the current direction of the electric antenna. If $E_z \neq 0$, this statement holds true only when the antenna intersects the plane perpendicular to the wave vector and thus $k_a = 0$. For other antenna directions during the spin period, the second term in (4) varies according to the variation of the $k_a$ component. Provided that the wave vector does not change during the spin period, this variation can be expressed,

$$k_a = k \sin\alpha\, \cos(2\pi f_s t), \tag{6}$$

where $k$ is the wave number, $f_s$ is the spin frequency, $t$ is time, and $\alpha$ is the angle deviation between $\mathbf{k}$ and the spin axis.

Practical application of (4) consists of measurements of the phase shift between $B_p$ and $E_a$ at a given frequency. This information can be either obtained from the $B_p$ waveform constructed with the magnetic vector samples and the actual directions of the electric antenna, or by combining the cross-spectra of $E_a$ with $B_x$ and $B_y$ components using an average antenna direction. The former procedure has been used in the present study, the latter one in the statistical analysis of emissions below $f_{\mathrm{H}+}$ [*Santolík and Parrot*, 1998]. In both cases, the resulting phase differences are calculated once in each time interval necessary for the spectral analysis. If the values of the $B_p$–$E_a$ phase are constant during the spin period, the first term in (4) is dominant and the phase difference should be either near to 0° ($k_z > 0$, downgoing waves), or 180° (upgoing waves with $k_z < 0$).

If the phase shift varies with a period equal to the spin, the second term in (4) becomes nonnegligible ($E_z \neq 0$). Then the values of the phase shift depend further on the mutual phase between $E_a$ and $E_z$. In any case the $B_p$–$E_a$ phase is fully determined by the $k_z$ sign two times per period, when $k_a = 0$. These moments are easy to identify in the temporal evolution of the phase shift, taking into account (6), and therefore it is possible to recognize the downgoing and upgoing waves even if $E_z \neq 0$. However, this latter case has not been observed in the present study.

**Acknowledgments.** Many thanks are due to B. Holback (IRF-U), the PI of the Freja wave experiment for the use of his data and for helpful discussions about the data handling. Data are available in France thanks to H. de Feraudy (CETP-UVSQ) who is Co-I of this experiment. Important software has been used for the data analysis in this paper: ISDAT (Interactive Science Data Analysis Tool) developed by A. Lundgren (IRF-U), and SWAN (Software for Waveform Analysis) developed by D. Lagoutte (LPCE). Discussions with J.L. Rauch (LPCE), V. Fiala and F. Jiříček (IAP/ASCR) are acknowledged. This work was supported by the French-Czech program Barrande No. 98039/98055, and by the international program of scientific cooperation (PICS) No. 469. O. Santolík acknowledges the support of the Czech Grant Agency grants 202/97/1122 and 202/97/P076, and the GAAS grant A3042601.

Michel Blanc thanks Tord Oscarsson and another referee for their assistance in evaluating this paper.

## References

Chust, T., and D. Le Quéau, Resonant absorption of downward propagating electromagnetic hiss, *J. Geophys. Res.*, *101*, 10695–10710, 1996.

FREJA Magnetic Field Experiment Team, Magnetic field experiment on the Freja satellite, *Space Sci. Rev.*, *70*, 465–482, 1994.

Gurnett, D. A., S.D. Shawhan, N.M. Brice, and R.L. Smith, Ion cyclotron whistlers, *J. Geophys. Res.*, *70*, 1665–1688, 1965.

Gurnett, D. A., and T. B. Burns, The low-frequency cutoff of ELF emissions, *J. Geophys. Res.*, *73*, 7437–7445, 1968.

Gurnett, D. A., and L. A. Frank, ELF noise bands associated with auroral electron precipitation, *J. Geophys. Res.*, *77*, 3411–3417, 1972.

Gurnett, D. A., R.L. Huff, J.D. Menietti, J.L.Burch, J.D. Winningham, and S.D. Shawhan, Correlated low-frequency electric and magnetic noise along the auroral field lines, *J. Geophys. Res.*, *89*, 8971–8985, 1984.

Gustafsson, G., M. André, L. Matson, and H. Koskinen, On waves below the local proton gyrofrequency in auroral acceleration regions, *J. Geophys. Res.*, *95*, 5889–5904, 1990.

Hayakawa, M., F. Lefeuvre, and J.L. Rauch, The direction finding aboard AUREOL-3 of ELF waves at frequency above and below the proton gyrofrequency, in *CNES-Results of the ARCAD-3 Project and of the Recent Programmes in Magnetospheric and Ionospheric Physics*, p. 499, Cepadues-Editions, Toulouse, France, 1985.

Heacock, R. R., Whistler-like pulsation events in the frequency range 20 to 200 Hz, *Geophys. Res. Lett.*, *1*, 77–79, 1974.

Holback, B., S.-E. Jansson, L. Ahlen, G. Lundgren, L. Lyngdal, S. Powell, and A. Meyer, The FREJA wave and plasma density experiment, *Space Sci. Rev.*, *70*, 577–592, 1994.

LaBelle, J., and R.A. Treumann, Poynting vector measurements of electromagnetic ion cyclotron waves in the plasmasphere, *J. Geophys. Res.*, *97*, 13789–13797, 1992.

Lagoutte, D., J.C. Cerisier, J.L. Plagnaud, J.P. Villain, and B. Forget, High latitude ionospheric electrostatic disturbance studied by means of the wavelet transform, *J. Atmos. Terr. Phys.*, *54*, 1283–1294, 1992.

Lefeuvre, F., and M. Parrot, The use of the spectral matrix in analysing the propagation characteristics of electromagnetic emissions, *Proceedings of Conference on Achievement of the IMS, Eur. Space Agency Spec. Publ., ESA SP-217*, 715–722, 1984.

Lefeuvre, F., Y. Marouan, M. Parrot, and J.L. Rauch, Rapid determination of the sense of polarization and propagation for random electromagnetic wave fields. Application to GEOS1 and AUREOL3 data, *Ann. Geophys.*, *4*, 457–468, 1986. (Correction, *Ann. Geophys.*, *5*, 251, 1987.)

Lefeuvre, F., J. L. Rauch, D. Lagoutte, J. J. Berthelier, and J. C. Cerisier, Propagation characteristics of dayside low-altitude hiss: Case studies, *J. Geophys. Res.*, *97*, 10601–10620, 1992.

Le Quéau, D., A. Roux, J. L. Rauch, F. Lefeuvre, and J. M. Bosqued, Heating of protons by resonant absorption in a multicomponent plasma, 2, Theoretical model, *J. Geophys. Res.*, *98*, 13363–13375, 1993.

Means, J. D., Use of the three-dimensional covariance matrix in analyzing the polarization properties of plane waves, *J. Geophys. Res.*, *77*, 5551–5559, 1972.

Muzzio, J. L. R., and J. J. Angerami, Ogo 4 observations of extremely low frequency hiss, *J. Geophys. Res.*, *77*, 1157–1173, 1972.

Mosier, S. R., Poynting flux studies of hiss with the INJUN 5 satellite, *J. Geophys. Res.*, *76*, 1713–1728, 1971.

Oscarsson, T., A. Vaivads, K. Rönnmark, J. H. Clemmons, H. de Feraudy, and B. Holback, Towards a consistent picture of the generation of electromagnetic ion cyclotron ELF waves on auroral field lines, *J. Geophys. Res.*, *102*, 24369–24386, 1997.

Pinçon, J. L., Y. Marouan, and F. Lefeuvre, Interpretation of measurements of the polarization percentage for plasma waves, *Ann. Geophys.*, *10*, 82–95, 1992.

Rauch, J.L., F. Lefeuvre, J.C. Cerisier, J.J. Berthelier, N. Boudko, G. Michailova, and O. Kapustina, Attenuation bands and cut off frequencies for ELF electromagnetic waves, in *CNES-Results of the ARCAD-3 Project and of the Recent Programmes in Magnetospheric and Ionospheric Physics*, p. 435, Cepadues-Editions, Toulouse, France, 1985.

Rauch, J.L., F. Lefeuvre, D. Le Quéau, A. Roux, J.M. Bosqued, and J.J. Berthelier, Heating of proton conics by resonant absorption in a multicomponent plasma, 1, Experimental evidence, *J. Geophys. Res.*, *98*, 13347–13361, 1993.

Saito, H., T. Yoshino, and N. Sato, Narrow-banded ELF emissions over the southern polar region, *Planet. Space Sci.*, *35*, 745–752, 1987.

Samson, J. C., and J. V. Olson, Some comments on the descriptions of the polarization states of waves, *Geophys. J. R. Astron. Soc.*, *61*, 115–129, 1980.

Santolík, O., and M. Parrot, Propagation analysis of electromagnetic waves between the helium and proton gyrofrequencies in the low-altitude auroral zone, *J. Geophys. Res.*, *103*, 20469–20480, 1998.

Smith, R. L., and N. M. Brice, Propagation in multicomponent plasmas, *J. Geophys. Res.*, *69*, 5029–5040, 1964.

Solomon, J., N. Cornilleau-Wehrlin, A. Korth, and G. Kremser, An experimental study of ELF/VLF hiss generation in the Earth's magnetosphere, *J. Geophys. Res.*, *93*, 1839–1847, 1988.

Stasiewicz, K., G. Gustafsson, G. Marklund, P.-A. Lindqvist, J. Clemmons, and L. Zanetti, Cavity resonators and Alfvén resonance cones observed on Freja, *J. Geophys. Res.*, *102*, 2565–2575, 1997.

Storey, L. R. O., and F. Lefeuvre, Theory for the interpretation of measurements of a random electromagnetic wave field in space, *Space Res.*, *14*, 381–386, 1974.

Storey, L. R. O., and F. Lefeuvre, The analysis of 6-component measurement of a random electromagnetic wave field in a magnetoplasma, 1, The direct problem, *Geophys. J. R. Astron. Soc.*, *56*, 255–270, 1979.

Storey, L. R. O., and F. Lefeuvre, The analysis of 6-component measurement of a random electromagnetic wave field in a magnetoplasma, 2, The integration kernels, *Geophys. J. R. Astron. Soc.*, *62*, 173–194, 1980.

Temerin, M., and R. L. Lysak, Electromagnetic ion cyclotron mode (ELF) waves generated by auroral electron precipitation, *J. Geophys. Res.*, *89*, 2849–2859, 1984.

Wahlund, J.-E., P. Louarn, T. Chust, H. de Feraudy, A. Roux, B. Holback, P.-O. Dovner, and G. Holmgren, On ion acoustic turbulence and the nonlinear evolution of kinetic Alfven waves in aurora, *Geophys. Res. Lett.*, *21*, 1831–1834, 1994.

Walker, D. N., P. K. Chaturvedi, M. Singh, P. Rodriguez, C. L. Siefring, and M. M. Baumack, Low-frequency oscillations associated with a polar cap auroral arc: Local spectral density estimation, *J. Geophys. Res.*, *96*, 3589–3600, 1991.

M. Parrot, Laboratoire de Physique et Chimie de l'Environnement, CNRS, 3A, Avenue de la Recherche Scientifique, 45071 Orléans cedex 02, France. (e-mail: mparrot@cnrs-orleans.fr)

O. Santolík, Faculty of Mathematics and Physics, Charles University, V Holešovičkách 2, CZ-18000 Praha 8, Czech Republic. (e-mail: ondrej.santolik@mff.cuni.cz)

(Received December 16, 1997; revised August 17, 1998;
accepted August 25, 1998.)